

Tuning phase transitions of FeSe thin flakes by field effect transistor with solid ion conductor as gate dielectric

B. Lei¹, N. Z. Wang¹, C. Shang¹, F. B. Meng¹, L. K. Ma¹, X. G. Luo^{1,4}, T. Wu^{1,4}, Z. Sun^{2,4},
Y. Wang⁵, Z. Jiang⁵, B. H. Mao⁶, Z. Liu^{6,7}, Y. J. Yu⁸, Y. B. Zhang^{4,8*} and X. H. Chen^{1,3,4†}

¹*Hefei National Laboratory for Physical Sciences at Microscale and Department of Physics,
and CAS Key Laboratory of Strongly-coupled Quantum Matter Physics,
University of Science and Technology of China, Hefei, Anhui 230026, China*

²*National Synchrotron Radiation Laboratory, University of Science and Technology of China, Hefei, Anhui 230026, China*

³*High Magnetic Field Laboratory, Chinese Academy of Sciences, Hefei, Anhui 230031, China*

⁴*Collaborative Innovation Center of Advanced Microstructures, Nanjing University, Nanjing 210093, China*

⁵*Shanghai Institute of Applied Physics, Chinese Academy of Sciences, Shanghai 201204, China*

⁶*State Key Laboratory of Functional Materials for Informatics, Shanghai Institute of Microsystem
and Information Technology, Chinese Academy of Sciences, Shanghai 200050, China*

⁷*School of Physical Science and Technology, Shanghai Tech University, Shanghai 200031, China*

⁸*State Key Laboratory of Surface Physics and Department of Physics, Fudan University, Shanghai 200433, China*

(Dated: September 27, 2016)

We develop a novel field effect transistor (FET) device using solid ion conductor (SIC) as a gate dielectric, and we can tune the carrier density of FeSe by driving lithium ions in and out of the FeSe thin flakes, and consequently control the material properties and its phase transitions. A dome-shaped superconducting phase diagram was mapped out with increasing Li content, with $T_c \sim 46.6$ K for the optimal doping, and an insulating phase was reached at the extremely overdoped regime. Our study suggests that, using solid ion conductor as a gate dielectric, the SIC-FET device can achieve much higher carrier doping in the bulk, and suit many surface sensitive experimental probes, and can stabilize novel structural phases that are inaccessible in ordinary conditions.

PACS numbers: 74.25.F-, 74.70.Xa, 74.78.-w

Chemical doping is a conventional way to introduce charge carriers into solids by replacing one of the constituent elements with another element of a different valence state. For instance, high temperature superconductivity is realized by suppressing the antiferromagnetism or spin density wave with chemical doping of 10% or 10^{21} dopant atoms per cm^3 in copper oxides and iron-based superconductors [1–3]. However, the chemical doping is incapable in many cases, because the element replacement and the variation of carrier density cannot practically cover a large regime and leave many phases unexplored. As a complementary method, the application of field effect transistors (FET) in two-dimensional systems is an effective way to control electronic properties via reversible changes of charge carrier density [4–18]. Such an electrostatic doping is desirable to study novel phases that cannot be achieved by material synthetic methods [7, 9–11, 13, 15, 16, 18]. For instance, we have utilized tunable ion intercalation with an ionic liquid to alter charge-ordered states in 1T-TaS₂ and induce phase transitions in thin flakes with reduced dimensionality [15]. The FET devices have been widely applied in the exploration of new superconductors [10, 11], the preparation for new devices [19, 20] as well as many applications in semiconductor industry [7].

So far, only two types of field effect transistor (FET) devices, metal-insulator-semiconductor (MIS) FET (Fig. 1(a)) and electric double layer (EDL) FET (Fig. 1(b)), can be widely used to continuously tune carrier density

[21, 22]. However, there are inherent drawbacks for the investigation of novel quantum phases in solids. In conventional MIS-FET devices, the electrostatic doping to a system is realized by the accumulation of mobile carriers at the surface of an insulator with a gate voltage applied [6, 7, 11, 21, 22]. A limited sheet carrier density n_{2D} of $\sim 1 \times 10^{13} \text{ cm}^{-2}$ can be obtained on the surface of an insulator before the gate dielectric breaks down due to the large electric field [5, 9, 11]. They cannot provide sufficient carriers to induce superconductivity [22]. The EDL-FET with a liquid electrolyte as a gate dielectric can achieve a higher two-dimensional carrier density n_{2D} of $\sim 8 \times 10^{14} \text{ cm}^{-2}$ [23]. However, the overlay of liquid electrolyte makes it difficult to suit the modern electronic technology and prevents heavily-doped electronic states from being characterized by many physical measurements. In addition, many materials of interest have electrochemical reaction with liquid electrolyte [24, 25]. Moreover, both of FETs can only tune the accumulation of carrier on the surface of materials. In this letter, using solid ion conductor as a gate dielectric, we introduce a new type of FET, SIC-FET (Fig. 1(c)). This type of FET devices solves the shortcoming of the carrier control methods mentioned above and can pave the way for the investigation of new electronic states in solids.

To demonstrate the capability of the SIC-FET device, we choose FeSe as a model material. FeSe has the simplest structure in iron-based high-temperature superconductors, with conducting FeSe layers stacked along c-axis

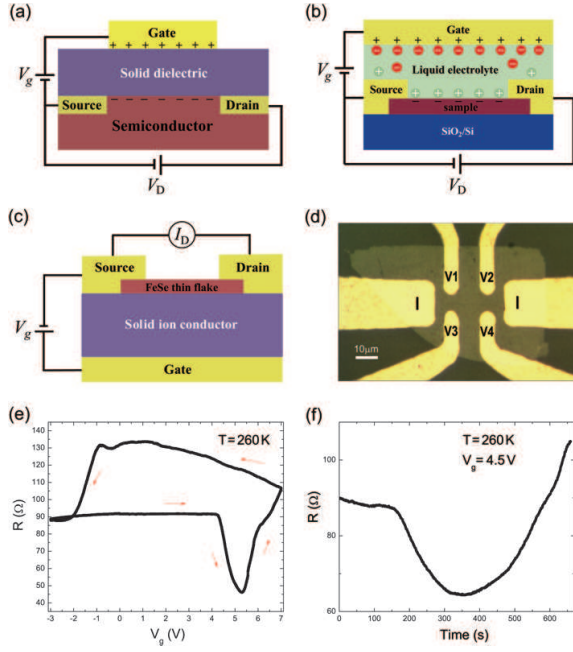


FIG. 1: (color online). Resistance controlled by gate voltage with SIC-FET device. (a) A schematic illustration of the MIS-FET with solid oxide such as SiO_2 or SrTiO_3 as the gate dielectric; (b) A schematic structure of EDL-FET with liquid electrolyte as the gate dielectric; (c) A schematic diagram of the SIC-FET device with the solid ion conductor as the gate dielectric; (d) The optical image of a FeSe thin flake with a standard Hall bar configuration with the current and voltage terminals labeled; (e) Gate voltage dependence of the resistance for a FeSe thin flake with typical thickness of about 18 nm in SIC-FET device. The continuously swept gate voltage with a scan rate of 2 mVs^{-1} was applied at 260 K; (f) The evolution of the resistance with time in SIC-FET with $V_g = 4.5 \text{ V}$ where the resistance of the sample started to drop.

[26]. FeSe and its derived superconductors are currently the focus of research in the field of iron-based superconductors [27–31]. In particular, the monolayer FeSe thin film on SrTiO_3 substrate has generated wide research interest because of its unexpected high- T_c superconductivity with T_c as high as 65 K, in sharp contrast to the bulk $T_c < 10 \text{ K}$ [27, 31–36]. Numerous studies have shown that those FeSe-derived materials with $T_c > 40 \text{ K}$ are heavily electron-doped systems, which share very similar electronic structures [37, 38]. The origin of superconductivity in these high- T_c materials remains to be an intriguing topic.

Recently, we have systematically tuned the superconductivity of FeSe thin flakes by electron doping with a FET device [39]. A onset high- T_c of 48 K was achieved in FeSe thin flakes with initial T_c less than 10 K. Intriguingly, a Lifshitz transition occurs at a certain carrier concentration, leading to a sudden change of T_c from less than 10 K to more than 30 K [39]. However, the superconducting regime in the carrier-doping phase di-

agram is incomplete due to the sample damage caused by electrochemical reactions between samples and ionic liquid at high gate voltage ($V_g > 6 \text{ V}$). To investigate the whole superconducting regime, a more effective method is required to introduce higher carrier density into FeSe.

Using the newly developed SIC-FET devices to increase electron doping in FeSe thin flakes by driving Li^+ ions into samples, we have found structural transitions from FeSe (11) phase to a low-doping $\text{Li}_y\text{Fe}_2\text{Se}_2$ (122 phase-I), then to a high-doping 122 phase-II. A dome-shaped superconducting phase diagram was mapped out with increasing Li content, and T_c is enhanced from 8 K in FeSe to 46.6 K for the optimal doping, then decreases in the overdoped regime and eventually an insulating phase emerges. The SIC-FET device proves to be able to introduce much higher carrier doping in bulk materials and stabilize novel structural phases. The application of such a novel FET device can provide exciting opportunities for exploring new quantum phases and new materials.

We prepared FET devices with the solid state lithium ion conductive glass ceramics as the gate dielectrics. The exfoliated FeSe thin flakes with a typical thickness of $\sim 18 \text{ nm}$ were used to fabricate the transport channel. Li^+ in the lithium ion conductor can move under the applied electric field. For positive gate voltage, Li^+ accumulates on the surface of samples, and then enters into samples to tune the carrier concentration. Figure 1(c) depicts a schematic illustration of the SIC-FET device. Detailed device preparation procedures are described in the Supplemental Material. Fig. 1(d) shows the optical image of a FeSe thin flake with a standard Hall bar configuration and with current and voltage terminals labeled. A continuously swept positive gate voltage with a scan rate of 2 mVs^{-1} was applied at 260 K, which is the optimal temperature for applying gate voltages. A typical R - V_g curve is shown in Fig. 1(e). The resistance of the FeSe thin flake remains almost unchanged with $V_g < 4.5 \text{ V}$, and starts to drop quickly for $V_g > 4.5 \text{ V}$, and reaches a minimum at 5.3 V, then increases rapidly. When the gate voltage is swept back to -2 V, the resistance can recover to the initial value. This behavior indicates that the tuning process is reversible. In fact, when the resistance of the sample starts to drop, the process of Li^+ intercalating into the FeSe thin flake sample will continue even if the gate voltage stays at a certain level. As shown in Fig. 1(f), a continuous change of the resistance of a sample in the relaxation process at a fixed gate voltage and temperature is quite similar to that with continuous sweeping of the gate voltage.

In FeSe-derived superconductors, numerous studies suggest that carrier concentration doped into FeSe layers is the primary factor that controls the superconducting transition temperature. When Li^+ ions in lithium ion conductor is driven to a FeSe thin flake with gating electric field, we can effectively introduce electron carri-

ers into FeSe layers. After intercalating Li^+ into FeSe thin flakes at 260 K, we quickly cooled down the FET devices to 210 K, below which the mobility of Li^+ ions in thin flake samples is completely suppressed. The gate voltage of 4.5 V, at which the resistance of sample starts to drop, was kept fixed during the whole measurements. In order to achieve a fine modulation of Li^+ ions intercalation, the FET device was relaxed at 260 K for a certain period of time before cooling down in each round. This procedure can lead to a series of doping levels with a controllable fashion.

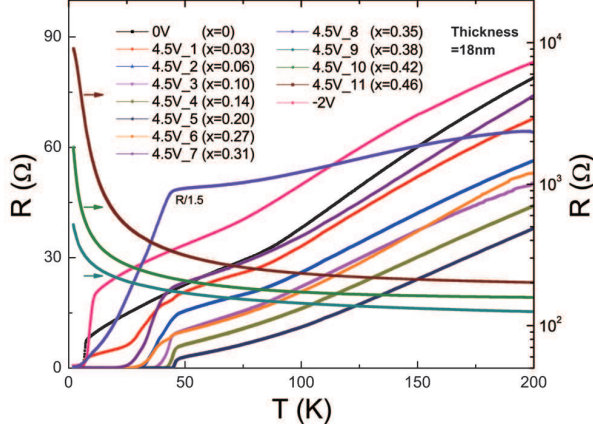


FIG. 2: (color online). Temperature dependence of resistance for a FeSe thin flake without gating and with gate voltage $V_g = 4.5$ V. The thickness of the thin flake determined by atomic force microscopy is 18 nm. The x is Li:Fe ratio whose determination is discussed in the Supplemental Material.

Using the four-terminal configuration, we measured a FeSe thin flake with various amounts of intercalated Li^+ ions below 200 K and show them in Fig. 2. At $V_g = 0$ V, the sample is superconducting with the onset critical temperature $T_c^{\text{onset}} = 7.3$ K and reaches zero-resistance at 5 K. Here, T_c^{onset} is defined as the intersection between the linear extrapolation of the normal state and the superconducting transition. With increasing the amount of intercalated Li^+ ions, the electronic carrier density of the sample increases (as shown in Fig. S2(b) of Supplemental Material), and the T_c as a function of Li^+ concentration shows a dome-like behavior. For the fifth round of cooling down at $V_g = 4.5$ V, the optimal superconductivity of the FeSe thin flake has been obtained with the Li/Fe ratio of 0.2. With further increasing the amount of intercalated Li^+ ions, the T_c starts to decrease, and eventually the FeSe thin flake shows an insulating behavior. When the gate voltage is swept back to -2 V, the resistance comes back to the initial value and the T_c also turns back to about 8 K, being almost the same as the initial T_c before gating. This behavior further indicates that the carrier tuning procedure with the SIC-FET device is reversible, though the evident higher resistance indicates that the intercalation of Li^+ ions into the system may damage

the sample in some way. We note here that both the optimal $T_c^{\text{onset}} = 46.6$ K and the transition from the superconductivity to insulating behavior were repeatable in every measured device. The sample with optimal doping exhibits $T_c^{\text{onset}} = 46.6$ K and zero-resistance temperature T_c^{zero} of 44.8 K, which is slightly higher than that of Li/ammonia intercalated FeSe synthesized by the ammonothermal method [29]. The width of the superconducting transition is less than 2 K, much sharper than that of ~ 13 K observed by tuning carrier concentration with EDL-FET device for FeSe thin flakes and thin films [39, 40] (see Fig. S3). This contrast suggests that the carrier concentration distribution in the SIC-FET devices is more homogeneous than that in the EDL-FET devices.

Owing to the small ionic radius of Li^+ ions, they can be easily intercalated into layered materials and alter local crystal structures of materials. Figure 3 shows the *in-situ* X-ray diffraction (XRD) patterns for a FeSe thin flake with thickness of 40 nm before and after the intercalation of Li^+ ions. Before the intercalation of Li^+ , the diffraction peak of (001) appears at $2\theta = 16.09^\circ$. With increasing the amount of intercalated Li^+ ions, the (001) peak intensity shows a drastic decrease with no noticeable variation in position. The phase with extremely low amount of Li^+ ions possesses the same structure as that of FeSe (11 phase), in which Li^+ ions diffuse randomly in the FeSe crystal. With the increase of Li^+ ions, two additional diffraction peaks appear at lower angles 13.76° and 13.29° , indicating new phases derived from the structure of FeSe. These new peaks do not belong to the same phase because only the 13.29° peak shows up in the insulating phase (see Fig. 3b). The data suggests that the intercalation of Li^+ ions into FeSe thin flakes results in two new phases.

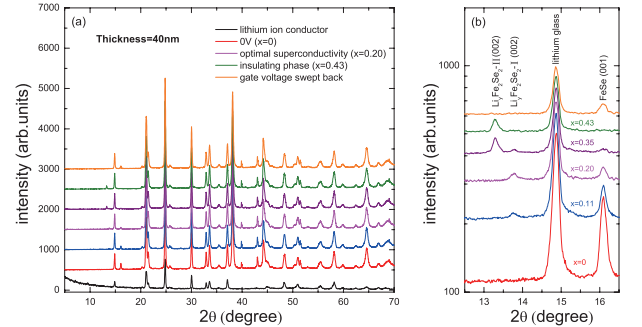


FIG. 3: (color online). *In-situ* X-ray diffraction (XRD) patterns for the FeSe thin flake in SIC-FET device before and after the intercalation of Li^+ ions. (a) The typical XRD patterns of the FeSe thin flakes with thickness of 40 nm for different charge stages; (b) The magnified view of the angle range from 12.5° to 16.5° .

To identify the phases with stronger signals, we carried out XRD measurements on a thicker flake of 150 nm. As shown in Fig. S5 in the Supplemental Material, two sets of (00 l) diffraction peaks have been identified,

suggesting that the separations between adjacent Fe layers (d) are 6.4128 Å and 6.6570 Å, respectively. In the $\text{Na}_{0.65}\text{Fe}_{1.93}\text{Se}_2$ and $\text{K}_x\text{Fe}_{2-y}\text{Se}_2$ of ThCr_2Si_2 -type structure, the separations between neighboring FeSe layers are 6.8339 Å and 7.0180 Å, respectively [27, 41]. Considering that the ionic radius of Li^+ is smaller than that of Na^+ and K^+ , we attribute the two new phases to the ThCr_2Si_2 -type structure. We label the phase with a smaller lattice parameter c (12.8256 Å) as $\text{Li}_y\text{Fe}_2\text{Se}_2$ -I (122-I) phase and the one with larger c (13.314 Å) as $\text{Li}_y\text{Fe}_2\text{Se}_2$ -II (122-II) phase. The different layer separation d in the two phases can be attributed to the different Li^+ contents. Generally speaking, the small cation may have more diverse arrangements and coordination environments. Similar multiple phases have been reported in Na-intercalated FeSe superconductors [41]. When the thin flake is tuned to an insulator, the 11 phase and 122-I phase completely disappear and only 122-II phase exists as shown in Fig. 3. When the gate voltage is swept back to -2 V, the 122-I and -II phases completely disappear, and the FeSe phase recovers. This result indicates that the newly formed 122 structural phases can only exist under the electric field, and also implies that the process of intercalating Li^+ into the FeSe controlled by electric field is reversible. We note that the two new Li-intercalated FeSe phases have not been reported before, which are induced and stabilized by the SIC-FET device. Since the superconductivity in bulk FeSe-derived materials is primarily determined by carrier concentration doped into FeSe layers, the emerging new 122 structures may not play a primary role in the novel electronic properties of FeSe layers. However, the superconductivity and other properties, and especially the insulating behavior of these new 122 phases is very intriguing for further investigation.

To acquire more details about the electron doping and structural modification, *in-situ* X-ray photoelectron spectroscopy (XPS) and X-ray absorption near edge spectra (XANES) were performed on the SIC-FET devices to study FeSe thin flakes with different lithium contents. The XPS result for Fe $2p$ is shown in Fig. S5. The spectrum taken on FeSe single crystals agrees well with that of the as-grown FeSe film [42]. It consists of two features at 706.6 eV and 707.8 eV. We use the center of the weight of the Fe $2p$ peaks to qualitatively describe the change of Fe chemical valence. The center point decreases from 707.1 eV (no gating), 707.0 eV (optimal superconductivity) and eventually to 706.6 eV (insulating phase). Clearly, the Fe valence state decreases with the increase of Li^+ ions intercalation. Due to the lack of reference data and surface sensitive nature of XPS, it is difficult for us to determine the Fe valence accurately at this moment. In addition, the XANES Fe K -edge spectra are shown in Fig. S6. This main absorption feature is due to the transition from Fe $1s$ to the $4p$ state. The absorption edge of the insulating phase FeSe thin flake shifts 2.5 eV

towards lower energy relative to that of pure FeSe, corresponding to a change of the Fe valence state from +2 in the pure FeSe to 1.23 ± 0.15 in the insulating phase. Furthermore, the slight parallel shift of absorption edge at the optimal superconducting state gives additional evidence for the random distribution of Li over Fe since a new local ordering may give rise to the deviations in the absorption spectra. On the other hand, the distinct shift of the absorption edge in the insulating phase from that of pure FeSe sample indicates a new ordering or structural change due to Li intercalation. Such a change is also responsible for the variation of the pronounced pre-edge feature at 7111 eV, which arises from the quadruple transition from Fe $1s$ to Fe $3d$. These findings support the formation of a new 122 structure phase in the insulating state. The decrease of Fe valence state observed in both of XPS and XANES suggests that Li^+ intercalation controlled by electric field is an effective method to introduce electron carriers into FeSe layers. The XANES results indicate that the Li is randomly distributed in 122-I phase, while is ordered in 122-II phase. Further investigation is required to determine Li positions and to reveal their microstructures in the two phases.

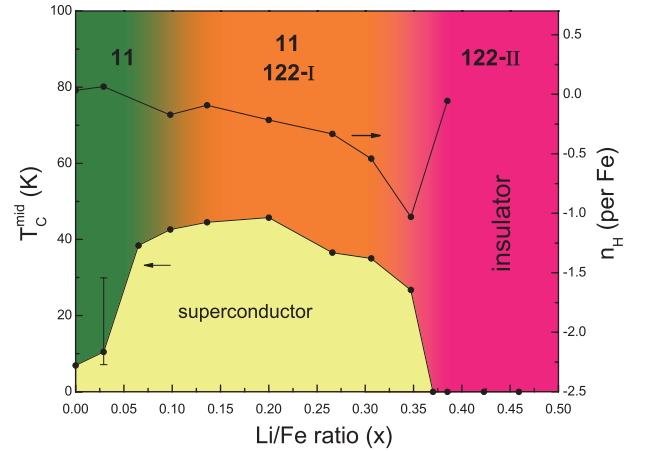


FIG. 4: (color online). The phase diagram of Li-intercalated FeSe thin flake as a function of Li/Fe ratio. The T_c shows a dome-like behavior with increasing Li/Fe ratio. A phase transition from superconductor to insulator happens around Li/Fe ratio of 0.37. A series of structural phase transitions from FeSe 11 phase to $\text{Li}_y\text{Fe}_2\text{Se}_2$ -I phase, then to $\text{Li}_y\text{Fe}_2\text{Se}_2$ -II phase takes place. The Hall number n_H is plotted to show the variation of carrier density.

The phase diagram of superconductivity and phase variations of Li^+ intercalated FeSe thin flakes are plotted as a function of Li/Fe ratio in Figure 4. The method of determining the amount of intercalated Li^+ content is described in the Supplemental Material. Based on the experimental results, the SIC-FET not only tunes the carrier concentration of the samples, but also modulates the crystal structure of materials. With increasing the amount of intercalated Li^+ , the T_c shows a dome-like be-

havior. The optimal superconductivity with mid-point critical temperature $T_c^{mid}=45.8$ K has been achieved when the Li/Fe ratio reaches 0.2. As the ratio is up to about 0.37, the superconductivity disappears completely, and then the sample becomes an insulator. A similar evolution from superconductor to insulator has been also observed in (Li,Fe)OHFeSe thin flake by electric field controlled lithium doping [43]. Most intriguingly, an abrupt jump of the T_c from ~ 10 K to ~ 40 K is observed when the Li/Fe ratio is around 0.07. Meanwhile, the Hall number n_H shows a corresponding sudden sign reversal. The evolution of Hall signal from hole-type to electron-type upon the increase of electron concentration induced by Li^+ intercalation can serve as an indicative of Lifshitz transition [44]. Similar transition has been observed in FeSe thin flakes with EDL-FET device [39]. However, for a comparison, the effective carrier concentration introduced by Li^+ intercalation can further increase and go beyond the upper limit of EDL-FET devices. As shown in Fig. 4, the carrier concentration suddenly decreases when the sample is tuned to an insulator, which could be attributed to some charge localization effect. In the whole phase diagram, the system experiences a series of phase transitions. In the beginning of Li^+ intercalation into FeSe thin flakes, the system keeps the same structure as FeSe, and a sudden enhancement of T_c occurs. With further increasing Li^+ intercalation, the 122-I phase emerges and coexists with the FeSe phase, then 122-II phase shows up at higher doping level. When the system is tuned to an insulator, FeSe phase and 122-I phase completely disappear, and only 122-II phase remains. We note that the coexistence of the 11, 122-I and -II phases is not intrinsic due to the inhomogeneity of the Li^+ distribution. Such inhomogeneous distribution of Li^+ in thin flakes strongly depends on the thickness of thin flakes, which was confirmed by the XRD patterns shown in Fig. 3 and Fig.S5 for thin flakes with different thickness of 40 nm and 150 nm, respectively. It should be pointed out that the data shown in Fig. 2 were obtained on the FeSe thin flakes of 18 nm, which should be much more homogeneous than that observed in Fig. 3. It is possible that no coexistence of the 11, 122-I and -II phases takes place in the devices with the flakes of 18 nm. We have tried to perform XRD measurements on the device with the 18 nm thin flakes by XRD, but the sample is too thin to detect signal. We thus selected a 40 nm FeSe thin flake for XRD characterization, which could inevitably involve inhomogeneity.

In summary, using solid lithium ion conductor as the gate dielectric, we developed a novel FET device (SIC-FET), which can effectively introduce electron carriers into layered materials. Compared to the MIS-FET and the EDL-FET devices, the SIC-FET device shows stronger capability of tuning carrier concentration, so that it can help to map out the phase diagram of FeSe over a wide range for the first time. Owing to the small

ionic radius of Li^+ , the SIC-FET device can tune the carrier concentration of entire materials with thickness of ten nanometers. Besides, the SIC-FET device can be used to search for new materials or novel superconductors with metastable structures. In particular, the configuration of SIC-FET devices is suitable for many other surface-sensitive experimental examinations. In our studies, two novel Li-intercalated FeSe phases with ThCr_2Si_2 -type structure, which cannot be synthesized by conventional methods, were obtained under the electric field. The investigation on the insulating $\text{Li}_y\text{Fe}_2\text{Se}_2$ -II phase could be helpful for the understanding of the superconducting mechanism for FeSe-derived superconductors. Our findings demonstrate the potential of the SIC-FET device to control superconductivity and to modulate the crystal structure, and open a new way to search for novel electronic or structural phases. Because of its significant advantage, the SIC-FET can serve in the modern electronic technology to some degree.

This work is supported by the National Natural Science Foundation of China (Grants No. 11190021, No. 11227902, No. 11534010 and No. 91422303), the Strategic Priority Research Program (B) of the Chinese Academy of Sciences (Grant No. XDB04040100), the National Key R&D Program of the MOST of China (Grant No. 2016YFA0300201), and the Hefei Science Center CAS (2016HSC-IU001).

* Electronic address: zhyb@fudan.edu.cn

† Electronic address: chenxh@ustc.edu.cn

- [1] J. G. Bednoz and K. A. Müller. Z. Phys. B **64**, 189-193 (1986).
- [2] Y. Kamihara *et al.*, J. Am. Chem. Soc. **130**, 3296-3297 (2008).
- [3] X. H. Chen *et al.*, Nature **453**, 761-762 (2008).
- [4] R. E. Glover *et al.*, Phys. Rev. Lett. **5**, 248-250 (1960).
- [5] C. H. Ahn *et al.*, Science **284**, 1152-1155 (1999).
- [6] D. Chiba *et al.*, Science **301**, 943 (2003).
- [7] C. H. Ahn *et al.*, Nature **424**, 1015-1018 (2003).
- [8] K. S. Novoselov *et al.*, Science **306**, 666 (2004).
- [9] A. D. Caviglia *et al.*, Nature **456**, 624-627 (2008).
- [10] K. Ueno *et al.*, Nat. Mater. **7**, 855 (2008).
- [11] K. Ueno *et al.*, Nat. Nanotechnol. **6**, 408 (2011).
- [12] J. T. Ye *et al.*, Nat. Mater. **9**, 125-128 (2010).
- [13] A. T. Bollinger *et al.*, Nature **472**, 458-460 (2011).
- [14] J. T. Ye *et al.*, Science **338**, 1193-1196 (2012).
- [15] Y. J. Yu *et al.*, Nat. Nanotechnol. **10**, 270 (2015).
- [16] Y. Saito *et al.*, Science **350**, 409-413 (2015).
- [17] J. M. Lu *et al.*, Science **350**, 1353-1357 (2015).
- [18] L. J. Li *et al.*, Nature **529**, 185-190 (2016).
- [19] B. Radisavljevic *et al.*, Nat. Nanotechnol. **6**, 147-150 (2011).
- [20] L. K. Li *et al.*, Nat. Nanotechnol. **9**, 372 (2014).
- [21] C. H. Ahn *et al.*, Rev. Mod. Phys. **78**, 1185-1212 (2006).
- [22] K. Ueno *et al.*, Journal of the Physical Society of Japan **83**, 032001 (2014).
- [23] H. T. Yuan *et al.*, Adv. Funct. Mater. **19**, 1046-1053 (2009).

- (2009).
- [24] J. Jeong *et al.*, Science **339**, 1402-1405 (2013).
 - [25] T. D. Schladt *et al.*, ACS Nano **7**, 8074-8081 (2013).
 - [26] F. C. Hsu *et al.*, Proc. Natl. Acad. Sci. USA **105**, 14262-14264 (2008).
 - [27] J. G. Guo *et al.*, Phys. Rev. B **82**, 180520(R) (2010).
 - [28] A. F. Wang *et al.*, Phys.Rev.B **83**, 060512(R) (2011).
 - [29] M. Burrard-Lucas *et al.*, Nat. Mater. **12**, 15-19 (2013).
 - [30] X. F. Lu, *et al.*, Nat. Mater. **14**, 325-329 (2015).
 - [31] Q. Y. Wang *et al.*, Chin. Phys. Lett. **29**, 037402 (2012).
 - [32] D. F. Liu *et al.*, Nat. Commun. **3**, 931 (2012).
 - [33] S. L. He *et al.*, Nat. Mater. **12**, 605-610 (2013).
 - [34] S. Y. Tan *et al.*, Nat. Mater. **12**, 634-640 (2013).
 - [35] R. Peng *et al.*, Nat. Commun. **5**, 5044 (2014).
 - [36] G-F. Ge *et al.*, Nat. Mater. **14**, 285-289 (2015).
 - [37] L. Zhao *et al.*, Nat. Commun. **7**, 10608 (2016).
 - [38] X. H. Niu *et al.*, Phys. Rev. B **92**, 060504(R) (2015).
 - [39] B. Lei *et al.*, Phys. Rev. Lett. **116**, 077002 (2016) .
 - [40] K. Hanzawa *et al.*, Proc. Natl. Acad. Sci. **113**, 3986-3990 (2016).
 - [41] J. Guo *et al.*, Nat. Commun. **5**, 4756 (2014)
 - [42] X. D. Qi *et al.*, Journal of Alloys and Compounds **509**, 6350-6353 (2011).
 - [43] B. Lei *et al.*, Phys. Rev. B **93**, 060501(R) (2016).
 - [44] I. M. Lifshitz, Sov. Phys. JETP **11**, 1130 (1960).